











Cite this: *Chem. Sci.*, 2022, 13, 13409

All publication charges for this article have been paid for by the Royal Society of Chemistry

# Correlations between experiments and simulations for formic acid oxidation†

Alexander Bagger, <sup>‡\*a</sup> Kim D. Jensen, <sup>‡a</sup> Maryam Rashedi, <sup>ab</sup> Rui Luo, <sup>ac</sup> Jia Du, <sup>d</sup> Damin Zhang, <sup>d</sup> Inês J. Pereira, <sup>a</sup> María Escudero-Escribano, <sup>aef</sup> Matthias Arenz <sup>ad</sup> and Jan Rossmeisl <sup>a</sup>

Electrocatalytic conversion of formic acid oxidation to CO<sub>2</sub> and the related CO<sub>2</sub> reduction to formic acid represent a potential closed carbon-loop based on renewable energy. However, formic acid fuel cells are inhibited by the formation of site-blocking species during the formic acid oxidation reaction. Recent studies have elucidated how the binding of carbon and hydrogen on catalyst surfaces promote CO<sub>2</sub> reduction towards CO and formic acid. This has also given fundamental insights into the reverse reaction, *i.e.* the oxidation of formic acid. In this work, simulations on multiple materials have been combined with formic acid oxidation experiments on electrocatalysts to shed light on the reaction and the accompanying catalytic limitations. We correlate data on different catalysts to show that (i) formate, which is the proposed formic acid oxidation intermediate, has similar binding energetics on Pt, Pd and Ag, while Ag does not work as a catalyst, and (ii) \*H adsorbed on the surface results in \*CO formation and poisoning through a chemical disproportionation step. Using these results, the fundamental limitations can be revealed and progress our understanding of the mechanism of the formic acid oxidation reaction.

Received 15th September 2022

Accepted 25th October 2022

DOI: 10.1039/d2sc05160e

rsc.li/chemical-science

## Introduction

Tremendous efforts are currently going into out-phasing fossil fuels in favor of sustainable fuels.<sup>1</sup> This is motivated by our need to close the carbon cycle<sup>2</sup> and pave the way for new fuel production routes.<sup>3</sup> Electrocatalytic technologies can in the future possibly allow direct electrification of chemical and fuel production. Examples include reduction of CO<sub>2</sub> towards CO, HCOOH, C<sub>2</sub>H<sub>4</sub>, C<sub>2</sub>H<sub>5</sub>OH and H<sub>2</sub>O towards H<sub>2</sub>.<sup>1</sup> Efficient fuel consumption through fuel cells (FCs) also holds great potential.<sup>4</sup> Liquid fuels such as formic acid and methanol have

attracted a lot of attention due to their viable energy density per mass- and volume, attractive handling/storage properties and potential uses in other non-fuel applications, *e.g.* as high value chemical building blocks for industry.<sup>3</sup>

Some liquid fuels, such as methanol, are notoriously limited in the oxidation toward CO<sub>2</sub> since the process goes through a CO intermediate.<sup>5</sup> CO oxidation then becomes the limiting factor determining the performance of direct methanol FCs (DMFCs). Formic acid as liquid fuel behaves differently; it has a CO<sub>2</sub>-like structure with two hydrogens attached. This molecular structure predicates that the oxidation process only requires the removal of two hydrogen atoms. Consequently, formic acid oxidation should ideally circumvent the problem of CO-poisoning.

To gauge formic acid's efficiency as a fuel we compare the single round trip efficiency of relevant closed-loop chemical compounds, *i.e.* hydrogen, formic acid, methanol and lithium batteries as seen in Table 1. Here we observe that the Li-battery storing and release of energy exhibits the highest efficiency followed by hydrogen. However, both Li-batteries and H<sub>2</sub> suffer from low energy density. Storing energy as methanol and formic acid is very similar in terms of the cost in electrolyzer energy. The major difference between formic acid and methanol arises when using the chemical in a fuel cell, where methanol is limited by CO oxidation.<sup>6</sup>

Depending on the  $U_{\text{FAOR}}$ , direct formic acid fuel cells (DFAFCs) can be considered an attractive alternative to

<sup>a</sup>University of Copenhagen, Department of Chemistry, Universitetsparken 5, 2100 Kbh-Ø, Denmark. E-mail: alexander@chem.ku.dk

<sup>b</sup>College of Science, University of Tehran, Enghelab Square, Tehran, Iran

<sup>c</sup>School of Environmental and Biological Engineering, Nanjing University of Science & Technology, Nanjing 210094, China

<sup>d</sup>University of Bern, Department of Chemistry, Biochemistry and Pharmaceutical Sciences, CH-3012 Bern, Switzerland

<sup>e</sup>Catalan Institute of Nanoscience and Nanotechnology (ICN2), CSIC, Barcelona Institute of Science and Technology, UAB Campus, 08193 Bellaterra, Barcelona, Spain

<sup>f</sup>ICREA, Pg. Lluís Companys 23, 08010 Barcelona, Spain

† Electronic supplementary information (ESI) available: Relevant aspects of the computational model and methods and the experimental methodology are included herein. (PDF). Additionally, atomic structures and analysis scripts are available on the webpage: [https://chem.ku.dk/research\\_sections/nanochem/theoretical-electrocatalysis/](https://chem.ku.dk/research_sections/nanochem/theoretical-electrocatalysis/). See DOI: <https://doi.org/10.1039/d2sc05160e>

‡ These authors contributed equally.



**Table 1** Estimated round-trip efficiencies ( $\eta = \frac{U_{\text{ORR}} - U_{\text{fuel cell reaction}}}{U_{\text{OER}} + U_{\text{electrolyzer reaction}}} \times 100\%$ ) calculated using the difference in energy potentials.

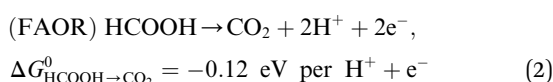
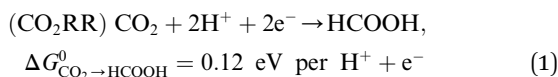
Common for hydrogen, formic acid, and methanol we use  $U_{\text{OER}} = 1.6 V_{\text{RHE}}$  and  $U_{\text{ORR}} = 0.8 V_{\text{RHE}}$

	Energy stored (electrolyzer)	Energy released (fuel cell)	Round trip efficiency, $\eta$
Hydrogen	$U_{\text{HER}} = -0.1 V_{\text{RHE}}$	$U_{\text{HOR}} = 0.1 V_{\text{RHE}}$	$\approx 41\%$
Formic acid	$U_{\text{CO}_2 \rightarrow \text{HCOOH}} = -0.8 V_{\text{RHE}}$	$U_{\text{FAOR}} = 0.2 V_{\text{RHE}}$	$\approx 25\%$
Methanol <sup>a</sup>	$U_{\text{CO}_2 \rightarrow \text{CO} + \text{H}_2} = -0.6 V_{\text{RHE}}$	$U_{\text{CO} \rightarrow \text{CO}_2} = 0.65 V_{\text{RHE}}$	$\approx 7\%$
Li-battery <sup>b</sup>			$\approx 90\%$

<sup>a</sup> Here only the cost of syngas production is considered, not the full formation of methanol. <sup>b</sup> Typical charge/discharge efficiency.

methanol fuel cells. Methanol provides 6 protons per reacted molecule and formic acid only two and therefore methanol has a  $\sim 3$  times higher volumetric energy density. However, the potential of a formic acid fuel cell is high; even a few hundred millivolts reduction in overpotential can allow formic acid to output more energy than methanol per molecule.

Key to understanding the limitation of formic acid oxidation is the direct link to the reverse electrochemical reaction, *i.e.* the  $\text{CO}_2$  reduction reaction ( $\text{CO}_2\text{RR}$ ).<sup>7,8</sup>  $\text{CO}_2\text{RR}$  to formic acid and the formic acid oxidation reaction (FAOR) can be written in the form:



where  $\Delta G^0$  is the thermodynamic potential per proton–electron pair of the reaction.

$\text{CO}_2\text{RR}$  selectivity is highly dependent on the catalyst material used and the crystal orientation.<sup>9–12</sup> Hori *et al.* showed that hydrogen is produced on Pt, Ru, Fe and Ni, carbon monoxide is produced on Au, Ag, Zn, Ga and Pd (with limited amounts of  $\text{H}_2$ ), and finally, formic acid is produced on Pb, In, Hg, Sn, Cd and Tl with almost 100% faradaic efficiency.<sup>11</sup> Importantly, hydrocarbons are uniquely produced on Cu.<sup>11</sup> Using simulations, we were able to classify the  $\text{CO}_2\text{RR}$  product distributions towards hydrogen, hydrocarbons, CO and formic acid due to the catalyst's affinity towards adsorbed  $^*\text{H}$  and  $^*\text{CO}$ .<sup>10</sup> Interestingly, we noted that the  $\text{CO}_2\text{RR}$  appears selective towards formic acid when weakening  $^*\text{H}$  binding (*i.e.* when there is no  $^*\text{H}$  on the catalyst surface). Moreover, from this study<sup>10</sup> we noted that the  $^*\text{OOCH}$  *vs.* the  $^*\text{COOH}$  intermediate cannot be used to distinguish the CO or formic acid product formation. Where previous works used  $^*\text{OOCH}$  as a descriptor for formic acid oxidation and  $^*\text{COOH}$  as a descriptor for CO production, and even recent discussion for  $\text{CO}_2$  reduction highlights the possible formic acid formation through  $^*\text{COOH}$ .<sup>13</sup> These findings and discussion are readily usable when considering the reverse reaction FAOR, which involves similar reaction intermediates to  $\text{CO}_2\text{RR}$  and *vice versa*.

FAOR exhibits the highest intrinsic activity on Pt and Pd.<sup>14–19</sup> However, the reaction is affected by high overpotential and

formation of various poisoning and site-blocking intermediates.<sup>20</sup> The following observations are reported in the literature, as also shown in ESI Fig. S1:† (i) FAOR onsets at low potentials does not necessarily correspond to high FAOR currents. (ii) Hysteresis between anodic and cathodic scans is a common occurrence, showing a higher current in cathodic scans than anodic ones, which shows that the reaction rate depends on the prehistory. Typically, this “memory effect” is related to unwanted reactions which form species that block the surface, *i.e.* poisoning species. (iii) Pt(111) is more active than Pd(100) in the low overpotential region; however, interestingly, this relationship shifts at higher potentials. (iv) As an observation it is known that there is a difference for Pt and Pd with respect to the CO poisoning during FAOR.<sup>8</sup> The ideal FAOR catalyst on the other hand should show reversible cyclic voltammetry (CV), high activity, low onset potential and stable currents, as illustrated in Fig. S2.†

To understand the mechanism of this important reaction numerous attempts have been made to map possible FAOR pathways,<sup>20–24</sup> which we illustrate by the literature study overview in Fig. 1. A dual-pathway mechanism for formic acid oxidation is established by the community.<sup>25,26</sup> The direct pathways, which leads to the desired final product of  $\text{CO}_2$  through the formate adsorption,<sup>27</sup> and another path where adsorbed CO, the poisoning species, is formed. The CO formation can be thought of as being formed through a so-called chemical disproportionation reaction, where an activated formic acid intermediate reacts with a hydrogen to form water and CO (*e.g.*  $^*\text{COOH} + ^*\text{H} \rightarrow ^*\text{CO} + \text{H}_2\text{O}$ ). However, the nature of the reactive intermediate in the direct pathway is still under strong debate and it is not given that it is the most stable intermediate (*e.g.*, formate) should also be the reaction intermediate. The community has focused on elucidating the reaction mechanism and attempted to circumvent poisoning issues: through pathway engineering,<sup>21,22</sup> changing electrolyte composition,<sup>23</sup> or inclusion of sites with the ability to remove poisoning or site-blocking species.<sup>24,28–30</sup> CO-poisoning from partial HCOOH oxidation is often considered the principal culprit<sup>28</sup> and various works suggest CO formation can be avoided utilizing a single/dual-site catalyst.<sup>31–34</sup> However, catalysts such as Au–Pt,<sup>21</sup> Pt–Hg/C<sup>35</sup> and Pd–Hg/C<sup>36</sup> exhibit limited catalytic improvement over their pure metal counterparts, for some overviews see Fig. S4 in ESI.† In this work, we will take a new



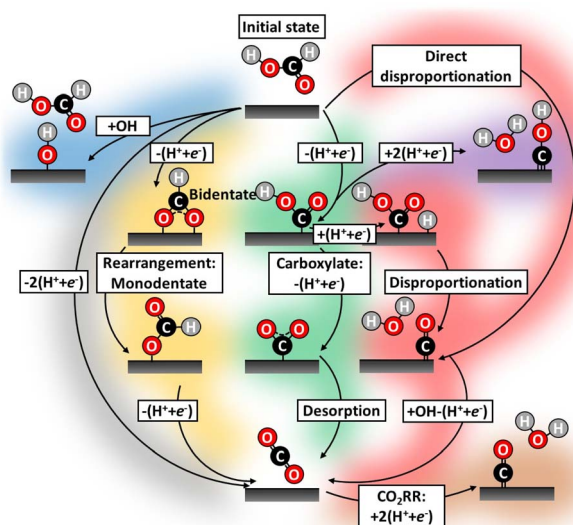


Fig. 1 Literature study highlighting all the conceived FAOR reaction pathways during potential cycling.<sup>38</sup> Historically, FAOR has been split into the direct (gray)<sup>39,40</sup> and indirect (green and yellow)<sup>16,39,41,42</sup> pathways. Further, partial FAOR and catalyst oxidation forming unwarranted surface blocking have been suggested, e.g.  $\text{CO}_x\text{H}_y$  species (purple),<sup>20,25,43</sup> CO (red)<sup>44</sup> and hydroxide/oxides (blue).<sup>38</sup> Even  $\text{CO}_2\text{RR}$  induced CO formation by applying too cathodic potential (brown)<sup>40</sup> have been suggested. Recently, formate (yellow)<sup>28,39,45,46</sup> in various arrangements has gained attention as potential catalyst site-blocking agents.

view on all possible pathways for working catalysts. We carry out electrochemical characterization on Pd/C and Pt/C catalyst as well as Pt–Hg/C,<sup>35</sup> Pd–Hg/C<sup>36</sup> and Pt–Bi/C,<sup>37</sup> following the protocols reported in the literature for the preparations of these catalysts. Furthermore, we try to validate the possible reaction path for not/low performing catalysts (e.g., Ag) for formic acid oxidation.

In this work, we address the following fundamental questions in FAOR:

(i) Is the FAOR activity correlated with the  $^*\text{COOH}$  or the  $^*\text{OOCH}$  intermediate?

(ii) How is CO formed during the FAOR?

To probe the scientific questions, we use a combination of experimental tools based on cyclic voltammetry (CV) and chronoamperometric (CA) and for simulations we use density functional theory (DFT) calculations on the binding of carboxyl,  $^*\text{COOH}$ , formate bidentate,  $^*\text{OOCH}$ , and hydrogen,  $^*\text{H}$ .

## Results and discussion

Fig. 2 summarizes experimental electrochemical data of Pt/C, Pd/C, Pt–Hg/C, Pd–Hg/C and Pt–Bi/C. Here we investigate only known and active FAOR catalyst, and both extended surfaces as Pt/C and Pd/C, but also single site catalyst Pt–Hg/C and Pd–Hg/C and the noteworthy very active Pt–Bi/C system. These investigated catalysts are synthesized from the same starting materials, *i.e.* pre-made Pd or Pt catalyst which we then modified by (electro)deposition of Hg or Bi at room temperature. Consequently, it is reasonable to expect that no significant impact of

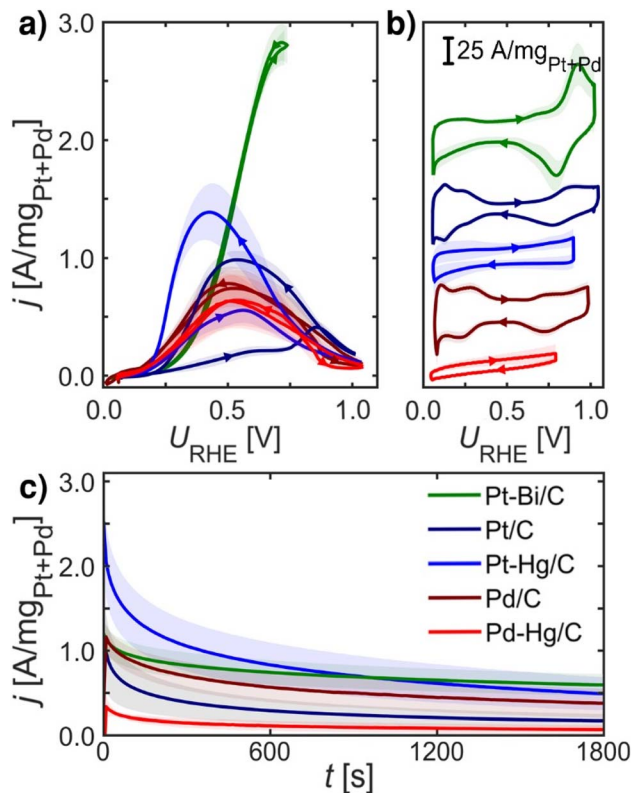


Fig. 2 Electrochemical data recorded at room temperature of equal loading nanoparticle catalysts: Pt/C (navy blue), Pd/C (crimson), Pt–Hg/C (blue), Pd–Hg/C (red) and Pt–Bi/C (green) systems on glassy carbon in Ar-saturated 0.1 M  $\text{HClO}_4$  with 0.1 M  $\text{HCOOH}$  at 1600 rpm, unless otherwise stated. (a) FAOR CVs at  $10 \text{ mV s}^{-1}$ . (b) Base CVs in Ar-saturated 0.1 M  $\text{HClO}_4$  at 400 rpm and  $50 \text{ mV s}^{-1}$ . (c) CA at  $0.55 V_{\text{RHE}}$  for 30 min. All measurements were repeated at least three times (shade represents standard deviation), *IR*-compensated and post-corrected, for experimental details see ESI and Fig. S5–S8.† Note, Pt–Bi/C was unstable at higher potentials (see ESI†) hence a reduced potential range was utilized.

the catalysts' surface area arises due to the modification, allowing for catalyst comparison. However, verifying this expectation using standard electrochemical surface area (ECSA) evaluation (e.g. utilizing  $^*\text{CO}$ -stripping or hydrogen under potential deposited, H-UPD, charges) is not possible as these species do not adsorb specifically on Hg and Bi modified catalysts.

Fig. 2a shows the formic acid oxidation CV during rotation and  $10 \text{ mV s}^{-1}$  scan-rate on the five catalysts. Fig. 2b depicts the base CVs exhibiting suppressed hydrogen underpotential deposition ( $\text{H}_{\text{UPD}}$ ) on the Pt–Bi/C, Pt–Hg/C and Pd–Hg/C compared to the Pd/C and Pt/C counterparts. Fig. 2c displays the formic acid oxidation CA at  $0.55 V_{\text{RHE}}$  for 30 min, illustrating the loss in activity at this potential due to the formation of poisoning or blocking species. For Pt/C and Pt–Hg/C, an apparent hysteresis is seen in the oxidation between the forward and backward scans of Fig. 2a indicating an irreversible change in the catalyst going to low potentials. Interestingly, taking a combined view on Fig. 2a and c shows that forming single-



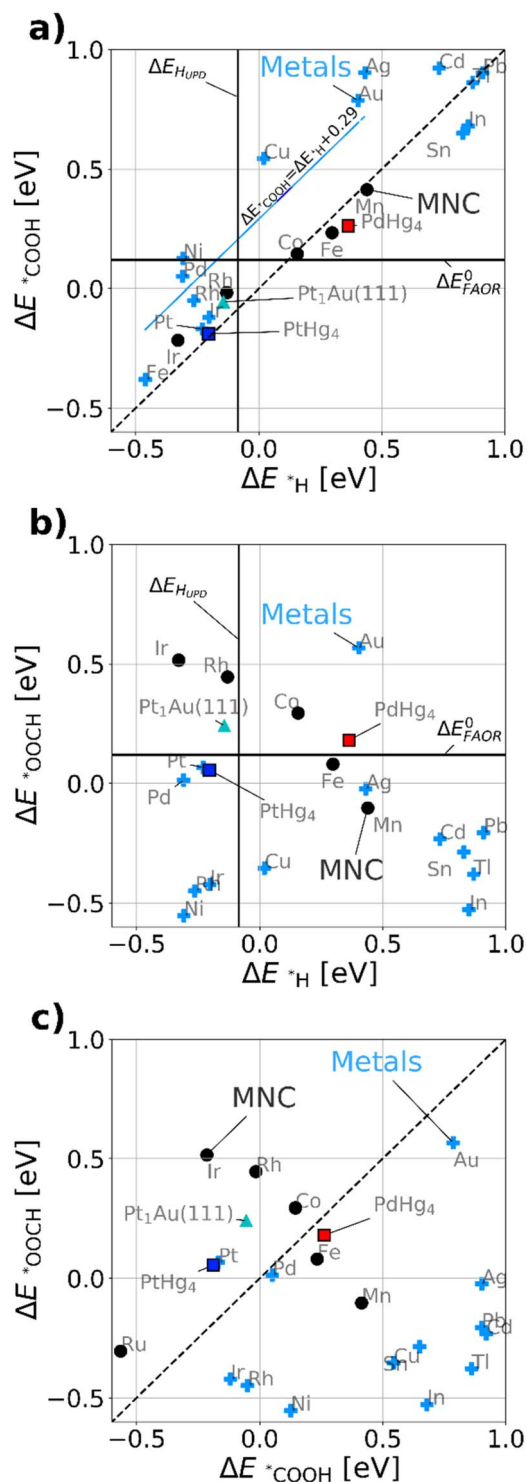


Fig. 3 DFT calculated binding energies for metal fcc(111) (light-blue crosses) and single-site catalyst. MNC-based (black points), Pt atom in Au(111) denoted Pt<sub>1</sub>Au(111) (cyan triangle), PdHg<sub>4</sub> (black/red square) and PtHg<sub>4</sub> (black/blue square). (a) \*COOH vs. \*H. (b) \*OOCH vs. \*H. (c) \*OOCH vs. \*COOH, here the dashed line shows the diagonal indication the affinity towards formate bound through carbon or oxygen. Here it is assumed  $\Delta E_{\text{FAOR}}^0 \approx \Delta G_{\text{FAOR}}^0$ . Further, we used CO<sub>2</sub> and H<sub>2</sub> for references when calculating \*COOH,  $\Delta E_{\text{FAOR}}^0$  is 0.12 eV per electron.

sites of Pt through Hg alloying<sup>35,36</sup> tend to improve the FAOR onset. In contrast, Pd-based catalysts generally do not exhibit any hysteresis. The Pt-Bi/C system exhibit the highest FAOR current with least hysteresis, but also with the highest overpotential. Additional relevant electrochemical studies can be found in the ESI,<sup>†</sup> represented through Fig. S10–S13.<sup>†</sup> To explain these observations in Fig. 2 we turned to DFT.

Fig. 3a maps out the DFT calculated \*COOH vs. \*H binding energies of the most relevant model metal (111) facets and single-site catalysts, such as MNCs, PtHg<sub>4</sub>,<sup>35</sup> PdHg<sub>4</sub> (ref. 36) and single Pt atoms in Au, Pt<sub>1</sub>Au(111)<sup>21</sup> (for computational details see ESI<sup>†</sup>). *Via* simulations we study both metals and the single-site-catalysts as they both have a linear scaling:  $\Delta E_{*COOH} = \Delta E_{*H} + b$ . However,  $b$  is about 0.29 eV as previously<sup>47</sup> observed for metals and 0.0 eV for single-site catalysts, respectively. This allows for a fundamental destabilization of \*H vs. \*COOH at the single-site catalyst motifs as compared to metals, which is beneficial for improved FAOR by limiting the

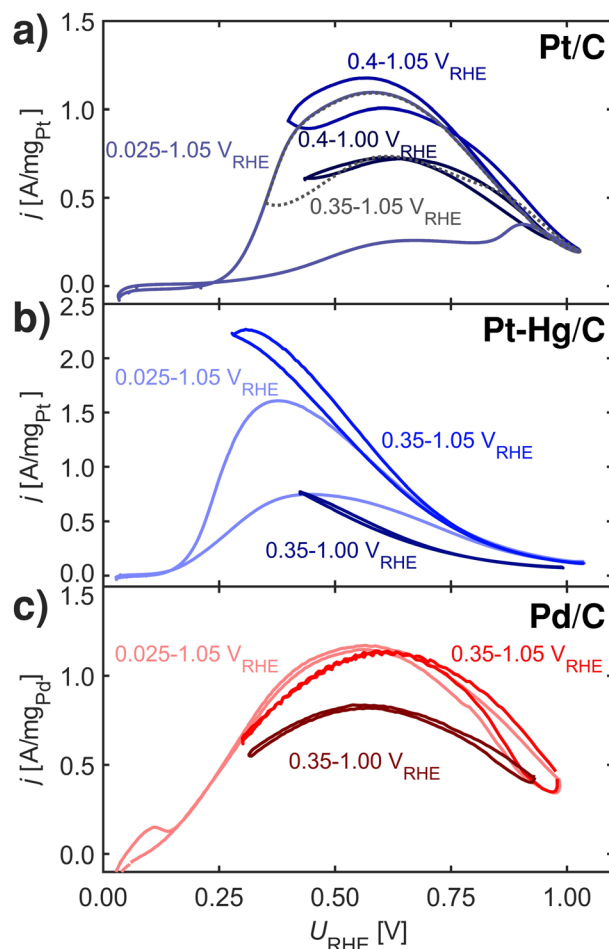


Fig. 4 FAOR CVs at 10 mV s<sup>-1</sup>, 1600 rpm and room temperature in Ar-saturated 0.1 M HClO<sub>4</sub> with 0.1 M HCOOH at different Pt potential limits. Ohmic drops were post-corrected. (a) Pt/C. (b) Pt-Hg/C. (c) Pd/C. Note, increasing lower potential limit minimizes the hysteresis in the CVs, lowering the upper potential limit generally decreases the activity. Note, that after cycling in the different potential limits returning to the full range of 0.025 to 1.05 V<sub>RHE</sub> re-initializes the FAOR response *i.e.* no irreversible changes arise due to dissolution or sintering.



disproportionation reaction. Besides the scaling, a vertical- and a horizontal line indicating  $H_{\text{UPD}}$  ( $\Delta E_{\text{HUPD}} = 0$  for  $1/2\text{H}_2 \leftrightarrow *H$ ) and formic acid's thermodynamic equilibrium potential have been included in Fig. 3a and b. Here it is assumed that  $\Delta E_{\text{FAOR}}^0 \approx \Delta G_{\text{FAOR}}^0$ , as thermodynamic corrections and water stabilization are expected to cancel out for the intermediates. The challenge to understand the implications of Fig. 3a is that one needs to compare  $*H$  as a reduction from  $\text{H}_2\text{O}$  and  $*\text{COOH}$  as oxidation from  $\text{HCOOH}$ . This means that  $*H$  stabilizes with negative potential, while  $*\text{COOH}$  stabilizes with positive potential during FAOR. Essentially, from Fig. 3a it can be inferred that materials to the left of approximately  $\Delta E_{\text{HUPD}}$  are limited by disproportionation at low potentials. While materials to the right are limited by weak binding  $*\text{COOH}$ . Most importantly, the fundamental scaling between  $*\text{COOH}$  and  $*H$  matter as adsorption of  $*H$  on the surface leads to the possibility of disproportionation towards CO. In conclusion, the single-atom catalyst scaling crosses the FAOR thermodynamic potential at values significantly above  $\Delta E_{\text{HUPD}}$ , which suggests that single-atom catalyst may work for FAOR near the FAOR equilibrium potential without carrying out the disproportionation reaction.

Fig. 3b displays the DFT calculated binding energies of  $*\text{OOCH}$  vs.  $*H$ . Conversely to Fig. 3a, there is no apparent scaling between formate bidentate and adsorbed hydrogen. However the oxygen bond for  $*\text{OOCH}$  scales with  $*OH$  and (bi)-carbonate ( $\text{HCO}_3/\text{CO}_3$ ), which have surface binding through oxygen. Carbonate species could be formed over time due to the equilibrium with  $\text{CO}_2$  and hence poisoning the surface, revealing a decaying activity as observed in Fig. 2c for all working FAOR catalysts. Investigating  $*\text{OOCH}$  as a function of  $*H$  is important as  $*\text{OOCH}$  has been suggested as an important reaction intermediate. Fig. 3b shows that the binding energy of the  $*\text{OOCH}$  intermediate on Ag is slightly too strong, but very close to the thermodynamic potential and similar to Pt and Pd. Essentially, if  $*\text{OOCH}$  was the important reaction intermediate for FAOR, then Ag should be working as FAOR catalyst at very low potential, and furthermore Ag does not suffer from disproportionation (as Ag  $*H$  binding far exceeds  $\Delta E_{\text{HUPD}}$ ). However, Ag is experimentally shown to be inert for the FAOR. The role of formate in the reaction is clearly a puzzle. For FAOR surface-enhanced IR absorption on Pt has experimentally confirmed formate on the surface<sup>27</sup> above  $0.7 V_{\text{RHE}}$  and further for  $\text{CO}_2\text{RR}$  *in situ* surface-enhanced Raman spectroscopy on Ag has experimentally confirmed formate on the surface.<sup>48</sup> As Pt converts formic acid to  $\text{CO}_2$  and Ag converts  $\text{CO}_2$  to CO, there seems no relation between the experimental observation of formate on the surface as reaction intermediate. We note that  $*\text{OOCH}$  scales with  $*OH$ , the  $*\text{OOCH}$  binding can be considered a probe of the oxidation affinity of the catalyst, *i.e.* having a strong  $*\text{OOCH}$  binding results in a lower oxidation potential.

Fig. 3c shows the  $*\text{OOCH}$  vs.  $*\text{COOH}$  binding for the catalyst, with a dashed line indicating the affinity towards carbon or oxygen. Depending on the catalyst we can see whether formate bidentate or carboxyl is favored. The working catalyst is Pt, which is well above the diagonal and Pd which is at the diagonal, while poorly working FAOR catalysts *e.g.* Ir<sup>49</sup> or Au<sup>50</sup> are slightly below the diagonal. Catalysts having stronger  $*\text{OOCH}$

binding vs.  $*\text{COOH}$  (below the diagonal), are basically oxidized before they can carry out FAOR.

The type of analysis illustrated in Fig. 3 is a powerful tool able to identify which catalyst suffers from disproportionation, poisoning or oxidation. By virtue of the  $*\text{COOH}$  vs.  $*H$  scaling-relations,<sup>10</sup> it gives fundamental insights into why literature historically has shown no significant FAOR activity at the thermodynamic potential for a metal catalysts. Implicitly Fig. 3a shows disproportionation occurring at low potential arising from the  $H_{\text{UPD}}$  and the consequent creation of  $*\text{CO}$  poisoning species. The creation of  $*\text{CO}$  leads to hysteresis between the anodic and cathodic sweeps in FAOR CVs. From this insight, one would expect that disproportionation is mitigated in the CVs by simply staying above  $H_{\text{UPD}}$  potentials.

Fig. 4 shows FAOR CVs of Pt/C, Pt-Hg/C and Pd/C cycled with varying potential limits. The potential ranges from 0.00–1.05  $V_{\text{RHE}}$  reveals that Pt/C and Pt-Hg/C are poisoned in anodic sweeps. While, changing to potentials, ranging from 0.40–1.05  $V_{\text{RHE}}$  for the Pt/C and 0.35–1.05  $V_{\text{RHE}}$  for the Pt-Hg/C, significantly increases the anodic activity. Hence, this allows us to indicate that  $H_{\text{UPD}}$  mediated disproportionation account for poisoning through CO on Pt catalysts. For Pd/C in Fig. 5c, decreasing the lower potential limit has no influence on the almost non-existing FAOR hysteresis. In this context, it is important to note that Pd is well-known to form Pd-hydride phases<sup>51</sup> below  $0.2 V_{\text{RHE}}$ , which then competes with  $*H$  adsorbed, *i.e.* at potentials relevant for both FAOR and  $\text{CO}_2\text{RR}$ . In relation to  $\text{CO}_2\text{RR}$ , we also note that Pd-hydride, leads to a high faradaic efficiency towards formate,<sup>52</sup> whereas at higher overpotentials CO and  $\text{H}_2$  will dominate.<sup>11</sup>

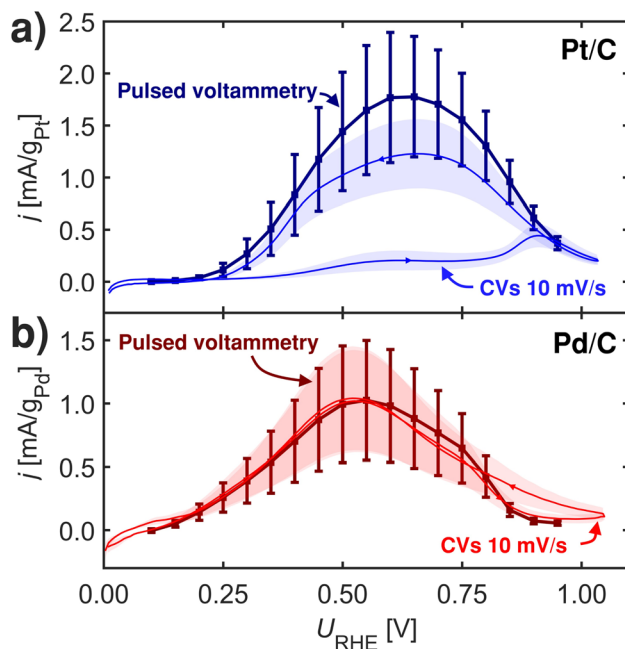


Fig. 5 2 s pulsed voltammetry and CVs at  $10 \text{ mV s}^{-1}$  at room-temperature at 1600 rpm in Ar-saturated 0.1 M  $\text{HClO}_4$  with 0.1 M  $\text{HCOOH}$ . (a) Pt/C. (b) Pd/C. Measurements repeated three times.



Concerning Fig. 4, one could erroneously assume that lowering the upper potential limit would not affect the CVs, while staying above the CO oxidation potential. This is however not the case, cycling 50 times from 0.35–1.00  $V_{\text{RHE}}$  reveals some form of deactivation of both Pt/C, Pt–Hg/C and Pd/C. We do not know what the origin of this deactivation is. Various studies reported in the literature suggests different reasons including deactivation to irreversible metal oxidation<sup>53,54</sup> due to insufficient surface reduction or accumulation of either  $^*\text{OOCH}$ ,<sup>55</sup>  $^*\text{COH}$ ,<sup>38</sup>  $^*\text{OCOH}$ <sup>56</sup> or  $^*\text{CO}$  species. Interesting is that *in situ* Fourier-transform infrared spectroscopy (FTIR) work<sup>57,58</sup> has shown that Pt, contrary to Pd, continuously form CO above  $H_{\text{UPD}}$  potential during FAOR.

Finding that  $^*\text{H}$  limits FAOR activity at low potential *via* disproportionation, allows one to hypothesize about the Pt–Bi and Pt–Hg systems, which perform better than Pt on two different perspectives. Pt–Bi shows no hysteresis and is active at higher overpotential as compared to Pt. The absence of a hysteresis in the CV indicates that Pt–Bi somehow circumvent the disproportionation reaction, potentially by blocking the surface for  $^*\text{H}$  at low potential as onset for Pt–Bi is higher than on Pt. Pt–Hg on the other hand is more active in the negative sweep, particular at lower potential, but does show clear hysteresis. Further we hypothesize that the Pt single-sites in Pt–Hg destabilizes  $^*\text{H}$  shifting the onset to lower potentials and increasing the activity at low potential, simply due to a limited disproportionation reaction.

To gauge how the FAOR is affected in the potentials regions above  $H_{\text{UPD}}$  we conducted pulsed voltammetry inspired by Clavilier *et al.*<sup>59</sup> In this type of pulsed voltammetry experiments, each potential investigated is separated by a surface re-initialization (at 1.05  $V_{\text{RHE}}$ ) cleaning the surface for all poisons through surface oxidation. The impact from dissolution at this oxidizing potential should be minimal.<sup>60,61</sup>

Fig. 5 shows pulsed voltammograms and corresponding CVs for Pt/C and Pd/C samples. Interestingly Pt/C becomes more active when pulsing, which is in contrast to Pd/C that does not show any changes from the pulsing. This experiment challenges  $^*\text{OOCH}$  species as site-blocking species. Since Pd has stronger relative  $^*\text{OOCH}$  to  $^*\text{COOH}$  binding than Pt, and it should hence be on Pd where activity was affected by blocking of  $^*\text{OOCH}$  species. One view for this observation could be given in the recent work by Koper and coworkers,<sup>8</sup> who noted that formate adsorption is important for formic acid oxidation, not as an active intermediate, but more as a self-protector against CO poisoning.

Beyond Pd and Pt catalyst, in Fig. 6, we tested Cu, Ni and Ag wires as FAOR catalyst. The experiments revealed that Ni indeed seems very active to oxidize either HCOOH or Ni. However, going to potentials above 0.2  $V_{\text{RHE}}$  tended to bring out a yellowish tinge in the electrolyte, and by looking into Ni's Pourbaix diagrams<sup>62</sup> it appears to readily dissolve as  $\text{Ni}^{2+}$  at 0.15  $V_{\text{RHE}}$  at pH 1, consequently making it a poor FAOR catalyst (unless there is some very narrow window that Ni is stable enough to oxidize HCOOH without dissolving). Similarly, Cu shows no FAOR activity only the well-known Cu oxidation current at potentials larger than 0.2  $V_{\text{RHE}}$  is observable. Ag is perhaps active towards FAOR but again this occur close to Ag

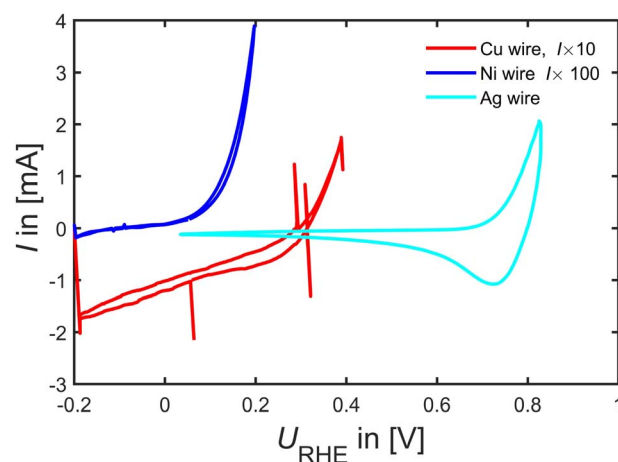


Fig. 6 FAOR data on a Cu, Ni and Ag wire at 50  $\text{mV s}^{-1}$  at room-temperature Ar-saturated 0.1 M  $\text{HClO}_4$  with 0.1 M HCOOH taken at 50  $\text{mV s}^{-1}$ .

dissolution potentials suggesting it to be a rather poor FAOR catalyst.

Most interesting when combining the observation of similar intermediate binding energetics in Fig. 3, we identified that Ag has similar binding energetics of formate as Pd and Pt, whereas Cu and Ni do not follow the energetic of Pd and Pt. Hence Cu and Ni can be used as test catalysts far from known working catalysts. However, as tested here in Fig. 6 there appears no significant FAOR on Ag, Cu and Ni.

## Conclusion

In conclusion we have correlated the FAOR activity with simulated DFT binding energies of  $^*\text{COOH}$ ,  $^*\text{OOCH}$  and  $^*\text{H}$  across multiple metal catalysts. We have observed that for an ideal catalyst, the FAOR equilibrium potential should be above its corresponding  $H_{\text{UPD}}$  potential in order to avoid the disproportionation. We found that  $^*\text{COOH}$  and  $^*\text{H}$  binding scale on both metal and single-site catalysts. This creates the fundamental limiting potential due to  $H_{\text{UPD}}$  mediated disproportionation on the surface. The carbon–hydrogen scaling is indeed a fundamental limitation, analog to the  $^*\text{OH}$  and  $^*\text{OOH}$  scaling for oxygen evolution and reduction. Experimentally, we show that a good performing FAOR catalyst should have the attributes of: (i) an onset close to the fundamental derived onset, (ii) no hysteresis between anodic- and cathodic CV scans and (iii) high and stable FAOR CA currents above the derived onsets fundamental limits. Interestingly, this works concludes on the direct relation between FAOR and  $\text{CO}_2\text{RR}$ ;  $^*\text{H}$  in combination with  $^*\text{COOH}$  forming CO in both FAOR and  $\text{CO}_2\text{RR}$ .

## Abbreviations

CA	Chronoamperometry
CV	Cyclic voltammogram/voltammetry
$\text{CO}_2\text{RR}$	$\text{CO}_2$ reduction reaction



DFAFC	Direct formic acid fuel cell
DMFC	Direct methanol fuel cell
DFT	Density functional theory
fcc	Face centered cubic
FAOR	Formic acid oxidation reaction
FC	Fuel cell
HER	Hydrogen evolution reaction
H <sub>UPD</sub>	Hydrogen underpotential deposition
MNC	Metal–nitrogen–carbon
OER	Oxygen evolution reaction
ORR	Oxygen reduction reaction
RHE	Reversible hydrogen electrode
ESI	Electronic supporting information

## Data availability

Data is available here: [https://nano.ku.dk/english/research/theoretical-electrocatalysis/katlabdb/formic\\_acid\\_oxidation\\_reaction/](https://nano.ku.dk/english/research/theoretical-electrocatalysis/katlabdb/formic_acid_oxidation_reaction/).

## Author contributions

The manuscript was written through the contributions of all authors. All authors have given approval to the final version of the manuscript.

## Conflicts of interest

There are no conflicts to declare.

## Acknowledgements

We would like to thank the Center for High Entropy Alloy Catalysis (CHEAC) funded by the Danish National Research Foundation (DNRF 149) and the Villum Foundation through the Villum Center for the Science of Sustainable Fuels and Chemicals (#9455) for funding this work. M. E.-E. and K. D. J. would like to thank the Independent Research Fund Denmark for the award of a DFF-Research Project 1 grant (9041-00224B). M. E.-E. acknowledges the Villum Foundation for financial support through a Villum Young Investigator Grant (project number: 19142). J. D. D. Z. would like to thank the funding from the China Scholarship Council (CSC). A. B would like to thank the Carlsberg foundation (CF21-0144).

## References

- Z. W. Seh, J. Kibsgaard, C. F. Dickens, I. Chorkendorff, J. K. Nørskov and T. F. Jaramillo, Combining Theory and Experiment in Electrocatalysis: Insights into Materials Design, *Science*, 2017, **355**(6321), eaad4998, DOI: [10.1126/science.aad4998](https://doi.org/10.1126/science.aad4998).
- S. C. Peter, Reduction of CO<sub>2</sub> to Chemicals and Fuels: A Solution to Global Warming and Energy Crisis, *ACS Energy Lett.*, 2018, **3**(7), 1557–1561, DOI: [10.1021/acscenergylett.8b00878](https://doi.org/10.1021/acscenergylett.8b00878).
- S. Cherevko, A. R. Zeradjanin, A. A. Topalov, N. Kulyk, I. Katsounaros and K. J. J. Mayrhofer, Dissolution of Noble Metals during Oxygen Evolution in Acidic Media, *ChemCatChem*, 2014, **6**(8), 2219–2223, DOI: [10.1002/cctc.201402194](https://doi.org/10.1002/cctc.201402194).
- B. C. Ong, S. K. Kamarudin and S. Basri, Direct Liquid Fuel Cells: A Review, *Int. J. Hydrogen Energy*, 2017, **42**(15), 10142–10157, DOI: [10.1016/j.ijhydene.2017.01.117](https://doi.org/10.1016/j.ijhydene.2017.01.117).
- T. Yajima, H. Uchida and M. Watanabe, In-Situ ATR-FTIR Spectroscopic Study of Electro-Oxidation of Methanol and Adsorbed CO at Pt-Ru Alloy, *J. Phys. Chem. B*, 2004, **108**(8), 2654–2659, DOI: [10.1021/jp037215q](https://doi.org/10.1021/jp037215q).
- D. S. Mekazni, R. M. Arán-Ais, A. Ferre-Vilaplana and E. Herrero, Why Methanol Electro-Oxidation on Platinum in Water Takes Place Only in the Presence of Adsorbed OH, *ACS Catal.*, 2022, 1965–1970, DOI: [10.1021/acscatal.1c05122](https://doi.org/10.1021/acscatal.1c05122).
- S. Nitopi, E. Bertheussen, S. B. Scott, X. Liu, A. K. Engstfeld, S. Horch, B. Seger, I. E. L. Stephens, K. Chan, C. Hahn, J. K. Nørskov, T. F. Jaramillo and I. Chorkendorff, Progress and Perspectives of Electrochemical CO<sub>2</sub> Reduction on Copper in Aqueous Electrolyte, *Chem. Rev.*, 2019, **119**(12), 7610–7672, DOI: [10.1021/acs.chemrev.8b00705](https://doi.org/10.1021/acs.chemrev.8b00705).
- X. Chen, L. P. Granda-Marulanda, I. T. McCrum and M. T. M. Koper, How Palladium Inhibits CO Poisoning during Electrocatalytic Formic Acid Oxidation and Carbon Dioxide Reduction, *Nat. Commun.*, 2022, **13**(1), 1–11, DOI: [10.1038/s41467-021-27793-5](https://doi.org/10.1038/s41467-021-27793-5).
- Y. Hori, I. Takahashi, O. Koga and N. Hoshi, Selective Formation of C<sub>2</sub> Compounds from Electrochemical Reduction of CO<sub>2</sub> at a Series of Copper Single Crystal Electrodes, *J. Phys. Chem. B*, 2002, **106**(1), 15–17, DOI: [10.1021/jp013478d](https://doi.org/10.1021/jp013478d).
- A. Bagger, W. Ju, A. S. Varela, P. Strasser and J. Rossmeisl, Electrochemical CO<sub>2</sub> Reduction: Classifying Cu Facets, *ACS Catal.*, 2019, **9**(9), 7894–7899, DOI: [10.1021/acscatal.9b01899](https://doi.org/10.1021/acscatal.9b01899).
- Y. Hori, H. Wakebe, T. Tsukamoto and O. Koga, Electrocatalytic Process of CO Selectivity in Electrochemical Reduction of CO<sub>2</sub> at Metal Electrodes in Aqueous Media, *Electrochim. Acta*, 1994, **39**(11–12), 1833–1839, DOI: [10.1016/0013-4686\(94\)85172-7](https://doi.org/10.1016/0013-4686(94)85172-7).
- P. Sebastián-Pascual, S. Mezzavilla, I. E. L. Stephens and M. Escudero-Escribano, Structure-Sensitivity and Electrolyte Effects in CO<sub>2</sub> Electroreduction: From Model Studies to Applications, *ChemCatChem*, 2019, **11**(16), 3626–3645, DOI: [10.1002/cctc.201900552](https://doi.org/10.1002/cctc.201900552).
- T. Zheng, C. Liu, C. Guo, M. Zhang, X. Li, Q. Jiang, W. Xue, H. Li, A. Li, C.-W. Pao, J. Xiao, C. Xia and J. Zeng, Copper-Catalysed Exclusive CO<sub>2</sub> to Pure Formic Acid Conversion via Single-Atom Alloying, *Nat. Nanotechnol.*, 2021, **16**(12), 1386–1393, DOI: [10.1038/s41565-021-00974-5](https://doi.org/10.1038/s41565-021-00974-5).
- M. Baldauf and D. M. Kolb, Formic Acid Oxidation on Ultrathin Pd Films on Au(Hkl) and Pt(Hkl) Electrodes, *J. Phys. Chem.*, 1996, **100**(27), 11375–11381, DOI: [10.1021/jp952859m](https://doi.org/10.1021/jp952859m).
- L. A. Kibler, A. M. El-Aziz, R. Hoyer and D. M. Kolb, Tuning Reaction Rates by Lateral Strain in a Palladium Monolayer,



- Angew. Chem., Int. Ed.*, 2005, **44**(14), 2080–2084, DOI: [10.1002/anie.200462127](https://doi.org/10.1002/anie.200462127).
- 16 A. Ferre-Vilaplana, J. V. Perales-Rondón, C. Buso-Rogero, J. M. Feliu and E. Herrero, Formic Acid Oxidation on Platinum Electrodes: A Detailed Mechanism Supported by Experiments and Calculations on Well-Defined Surfaces, *J. Mater. Chem. A*, 2017, **5**(41), 21773–21784, DOI: [10.1039/c7ta07116g](https://doi.org/10.1039/c7ta07116g).
- 17 T. Shen, S. Chen, R. Zeng, M. Gong, T. Zhao, Y. Lu, X. Liu, D. Xiao, Y. Yang, J. Hu, D. Wang, H. L. Xin and H. D. Abrunã, Tailoring the Antipoisoning Performance of Pd for Formic Acid Electrooxidation via an Ordered PdBi Intermetallic, *ACS Catal.*, 2020, **10**(17), 9977–9985, DOI: [10.1021/acscatal.0c01537](https://doi.org/10.1021/acscatal.0c01537).
- 18 R. Rizo and B. Roldan Cuenya, Shape-Controlled Nanoparticles as Anodic Catalysts in Low-Temperature Fuel Cells, *ACS Energy Lett.*, 2019, **4**(6), 1484–1495, DOI: [10.1021/acsenergylett.9b00565](https://doi.org/10.1021/acsenergylett.9b00565).
- 19 E. Plaza-Mayoral, I. J. Pereira, K. Nicole Dalby, K. D. Jensen, I. Chorkendorff, H. Falsig, P. Sebastián-Pascual and M. Escudero-Escribano, Pd–Au Nanostructured Electrocatalysts with Tunable Compositions for Formic Acid Oxidation, *ACS Appl. Energy Mater.*, 2022, **5**(9), 10632–10644, DOI: [10.1021/acsaem.2c01361](https://doi.org/10.1021/acsaem.2c01361).
- 20 A. Capon and R. Parsons, The Oxidation of Formic Acid at Noble Metal Electrodes Part 4. Platinum + Palladium Alloys, *J. Electroanal. Chem.*, 1975, **65**(1), 285–305, DOI: [10.1016/0368-1874\(75\)85124-0](https://doi.org/10.1016/0368-1874(75)85124-0).
- 21 P. N. Duchesne, Z. Y. Li, C. P. Deming, V. Fung, X. Zhao, J. Yuan, T. Regier, A. Aldalbahi, Z. Almarhoon, S. Chen, D. Jiang, N. Zheng and P. Zhang, Golden Single-Atomic-Site Platinum Electrocatalysts, *Nat. Mater.*, 2018, **17**(11), 1033–1039, DOI: [10.1038/s41563-018-0167-5](https://doi.org/10.1038/s41563-018-0167-5).
- 22 J. M. Feliu and E. Herrero, Formic Acid Oxidation, *Handb. Fuel Cells*, 2010, DOI: [10.1002/9780470974001.f206048](https://doi.org/10.1002/9780470974001.f206048).
- 23 J. Joo, T. Uchida, A. Cuesta, M. T. M. M. Koper and M. Osawa, Importance of Acid-Base Equilibrium in Electrocatalytic Oxidation of Formic Acid on Platinum, *J. Am. Chem. Soc.*, 2013, **135**(27), 9991–9994, DOI: [10.1021/ja403578s](https://doi.org/10.1021/ja403578s).
- 24 N. M. Marković, H. A. Gasteiger, P. N. Ross, X. Jiang, I. Villegas and M. J. Weaver, Electro-Oxidation Mechanisms of Methanol and Formic Acid on Pt–Ru Alloy Surfaces, *Electrochim. Acta*, 1995, **40**(1), 91–98, DOI: [10.1016/0013-4686\(94\)00241-R](https://doi.org/10.1016/0013-4686(94)00241-R).
- 25 A. Capon and R. Parsons, The Oxidation of Formic Acid at Noble Metal Electrodes Part III. Intermediates and Mechanism on Platinum Electrodes, *J. Electroanal. Chem.*, 1973, **45**(2), 205–231, DOI: [10.1016/S0022-0728\(73\)80158-5](https://doi.org/10.1016/S0022-0728(73)80158-5).
- 26 A. Betts, V. Briega-Martos, A. Cuesta and E. Herrero, Adsorbed Formate Is the Last Common Intermediate in the Dual-Path Mechanism of the Electrooxidation of Formic Acid, *ACS Catal.*, 2020, **10**(15), 8120–8130, DOI: [10.1021/acscatal.0c00791](https://doi.org/10.1021/acscatal.0c00791).
- 27 A. Miki, S. Ye and M. Osawa, Surface-Enhanced IR Absorption on Platinum Nanoparticles: An Application to Real-Time Monitoring of Electrocatalytic Reactions, *Chem. Commun.*, 2002, **2**(14), 1500–1501, DOI: [10.1039/b203392e](https://doi.org/10.1039/b203392e).
- 28 A. Ferre-Vilaplana, J. V. Perales-Rondón, J. M. Feliu and E. Herrero, Understanding the Effect of the Adatoms in the Formic Acid Oxidation Mechanism on Pt(111) Electrodes, *ACS Catal.*, 2015, **5**(2), 645–654, DOI: [10.1021/cs501729j](https://doi.org/10.1021/cs501729j).
- 29 J. V. Perales-Rondón, A. Ferre-Vilaplana, J. M. Feliu and E. Herrero, Oxidation Mechanism of Formic Acid on the Bismuth Adatom-Modified Pt(111) Surface, *J. Am. Chem. Soc.*, 2014, **136**(38), 13110–13113, DOI: [10.1021/ja505943h](https://doi.org/10.1021/ja505943h).
- 30 N. M. Marković and P. N. Ross Jr, Surface Science Studies of Model Fuel Cell Electrocatalysts, *Surf. Sci. Rep.*, 2002, **45**(4), 117–229, DOI: [10.1016/S0167-5729\(01\)00022-X](https://doi.org/10.1016/S0167-5729(01)00022-X).
- 31 Á. Cuesta, M. Escudero-Escribano, B. Lanova and H. Baltruschat, Cyclic Voltammetry, FTIRS, and DEMS Study of the Electrooxidation of Carbon Monoxide, Formic Acid, and Methanol on Cyanide-Modified Pt(111) Electrodes, *Langmuir*, 2009, **25**(11), 6500–6507, DOI: [10.1021/la8041154](https://doi.org/10.1021/la8041154).
- 32 K. Jiang, H. X. Zhang, S. Zou and W. B. Cai, Electrocatalysis of Formic Acid on Palladium and Platinum Surfaces: From Fundamental Mechanisms to Fuel Cell Applications, *Phys. Chem. Chem. Phys.*, 2014, **16**(38), 20360–20376, DOI: [10.1039/c4cp03151b](https://doi.org/10.1039/c4cp03151b).
- 33 A. Cuesta, At Least Three Contiguous Atoms Are Necessary for CO Formation during Methanol Electrooxidation on Platinum, *J. Am. Chem. Soc.*, 2006, **128**(41), 13332–13333, DOI: [10.1021/ja0644172](https://doi.org/10.1021/ja0644172).
- 34 W. Zhong, Y. Qi and M. Deng, The Ensemble Effect of Formic Acid Oxidation on Platinum-Gold Electrode Studied by First-Principles Calculations, *J. Power Sources*, 2015, **278**, 203–212, DOI: [10.1016/j.jpowsour.2014.12.071](https://doi.org/10.1016/j.jpowsour.2014.12.071).
- 35 S. Siahrostami, A. Verdager-Casadevall, M. Karamad, D. Deiana, P. Malacrida, B. Wickman, M. Escudero-Escribano, E. Paoli, R. Frydendal, T. W. Hansen, I. Chorkendorff, I. E. L. Stephens and J. Rossmeisl, Enabling Direct H<sub>2</sub>O<sub>2</sub> Production through Rational Electrocatalyst Design, *Nat. Mater.*, 2013, **12**(12), 1137–1143, DOI: [10.1038/nmat3795](https://doi.org/10.1038/nmat3795).
- 36 A. Verdager-Casadevall, D. Deiana, M. Karamad, S. Siahrostami, P. Malacrida, T. W. Hansen, J. Rossmeisl, I. Chorkendorff and I. E. L. Stephens, Trends in the Electrochemical Synthesis of H<sub>2</sub>O<sub>2</sub>: Enhancing Activity and Selectivity by Electrocatalytic Site Engineering, *Nano Lett.*, 2014, **14**(3), 1603–1608, DOI: [10.1021/nl500037x](https://doi.org/10.1021/nl500037x).
- 37 A. Sáez, E. Expósito, J. Solla-Gullón, V. Montiel and A. Aldaz, Bismuth-Modified Carbon Supported Pt Nanoparticles as Electrocatalysts for Direct Formic Acid Fuel Cells, *Electrochim. Acta*, 2012, **63**, 105–111, DOI: [10.1016/j.electacta.2011.12.076](https://doi.org/10.1016/j.electacta.2011.12.076).
- 38 S. G. Sun, J. Clavilier and A. Bewick, The Mechanism of Electrocatalytic Oxidation of Formic Acid on Pt (100) and Pt (111) in Sulphuric Acid Solution: An Emirs Study, *J. Electroanal. Chem.*, 1988, **240**(1–2), 147–159, DOI: [10.1016/0022-0728\(88\)80319-X](https://doi.org/10.1016/0022-0728(88)80319-X).
- 39 W. Gao, J. A. Keith, J. Anton and T. Jacob, Theoretical Elucidation of the Competitive Electro-Oxidation Mechanisms of Formic Acid on Pt(111), *J. Am. Chem. Soc.*, 2010, **132**(51), 18377–18385, DOI: [10.1021/ja1083317](https://doi.org/10.1021/ja1083317).





- 40 C. Rice, S. Ha, R. I. Masel and A. Wieckowski, Catalysts for Direct Formic Acid Fuel Cells, *J. Power Sources*, 2003, **115**(2), 229–235, DOI: [10.1016/S0378-7753\(03\)00026-0](https://doi.org/10.1016/S0378-7753(03)00026-0).
- 41 N. V. Rees and R. G. Compton, Sustainable Energy: A Review of Formic Acid Electrochemical Fuel Cells, *J. Solid State Electrochem.*, 2011, **15**(10), 2095–2100, DOI: [10.1007/s10008-011-1398-4](https://doi.org/10.1007/s10008-011-1398-4).
- 42 M. Neurock, M. Janik and A. Wieckowski, A First Principles Comparison of the Mechanism and Site Requirements for the Electrocatalytic Oxidation of Methanol and Formic Acid over Pt, *Faraday Discuss.*, 2009, **140**, 363–378, DOI: [10.1039/b804591g](https://doi.org/10.1039/b804591g).
- 43 X. H. Xia and T. Iwasita, Influence of Underpotential Deposited Lead upon the Oxidation of HCOOH in HClO<sub>4</sub> at Platinum Electrodes, *J. Electrochem. Soc.*, 1993, **140**(9), 2559–2565, DOI: [10.1149/1.2220862](https://doi.org/10.1149/1.2220862).
- 44 A. Tripković, K. Popović and R. Adžić, Structural Effects in Electrocatalysis: Oxidation of Formic Acid on Single Crystal Platinum Electrodes and Evidence for Oscillatory Behaviour, *J. Chim. Phys.*, 1991, **88**, 1635–1647, DOI: [10.1051/jcp/1991881635](https://doi.org/10.1051/jcp/1991881635).
- 45 J. Joo, T. Uchida, A. Cuesta, M. T. M. Koper and M. Osawa, The Effect of PH on the Electrocatalytic Oxidation of Formic Acid/Formate on Platinum: A Mechanistic Study by Surface-Enhanced Infrared Spectroscopy Coupled with Cyclic Voltammetry, *Electrochim. Acta*, 2014, **129**, 127–136, DOI: [10.1016/j.electacta.2014.02.040](https://doi.org/10.1016/j.electacta.2014.02.040).
- 46 M. R. Gennero de Chialvo, G. C. Luque and A. C. Chialvo, Formic Acid Electrooxidation on Platinum, Resolution of the Kinetic Mechanism in Steady State and Evaluation of the Kinetic Constants, *ChemistrySelect*, 2018, **3**(34), 9768–9772, DOI: [10.1002/slct.201801725](https://doi.org/10.1002/slct.201801725).
- 47 A. Bagger, W. Ju, A. S. Varela, P. Strasser and J. Rossmeisl, Single Site Porphyrin-like Structures Advantages over Metals for Selective Electrochemical CO<sub>2</sub> Reduction, *Catal. Today*, 2017, **288**, 74–78, DOI: [10.1016/j.cattod.2017.02.028](https://doi.org/10.1016/j.cattod.2017.02.028).
- 48 D. Bohra, I. Ledezma-Yanez, G. Li, W. de Jong, E. A. Pidko and W. A. Smith, Lateral Adsorbate Interactions Inhibit HCOO<sup>-</sup> While Promoting CO Selectivity for CO<sub>2</sub> Electrocatalysis on Silver, *Angew. Chem., Int. Ed.*, 2019, **58**(5), 1345–1349, DOI: [10.1002/anie.201811667](https://doi.org/10.1002/anie.201811667).
- 49 R. Gómez and M. J. Weaver, Electrochemical Infrared Studies of Monocrystalline Iridium Surfaces. 3. Adsorbed Nitric Oxide and Carbon Monoxide as Probes of Ir(100) Interfacial Structure, *J. Phys. Chem. B*, 1998, **102**(19), 3754–3764, DOI: [10.1021/jp980098s](https://doi.org/10.1021/jp980098s).
- 50 A. Cuesta, G. Cabello, F. W. Hartl, M. Escudero-Escribano, C. Vaz-Domínguez, L. A. Kibler, M. Osawa and C. Gutiérrez, Electrooxidation of Formic Acid on Gold: An ATR-SEIRAS Study of the Role of Adsorbed Formate, *Catal. Today*, 2013, **202**(1), 79–86, DOI: [10.1016/j.cattod.2012.04.022](https://doi.org/10.1016/j.cattod.2012.04.022).
- 51 A. Rose, S. Maniguet, R. J. Mathew, C. Slater, J. Yao and A. E. Russell, Hydride Phase Formation in Carbon Supported Palladium Nanoparticle Electrodes Investigated Using *in Situ* EXAFS and XRD, *Phys. Chem. Chem. Phys.*, 2003, **5**(15), 3220–3225, DOI: [10.1039/b302956e](https://doi.org/10.1039/b302956e).
- 52 D. Gao, H. Zhou, F. Cai, D. Wang, Y. Hu, B. Jiang, W. B. Cai, X. Chen, R. Si, F. Yang, S. Miao, J. Wang, G. Wang and X. Bao, Switchable CO<sub>2</sub> Electroreduction *via* Engineering Active Phases of Pd Nanoparticles, *Nano Res.*, 2017, **10**(6), 2181–2191, DOI: [10.1007/s12274-017-1514-6](https://doi.org/10.1007/s12274-017-1514-6).
- 53 J. M. Tura, P. Regull, L. Victori and M. D. de Castellar, XPS and IR (ATR) Analysis of Pd Oxide Films Obtained by Electrochemical Methods, *Surf. Interface Anal.*, 1988, **11**(8), 447–449, DOI: [10.1002/sia.740110807](https://doi.org/10.1002/sia.740110807).
- 54 V. A. Saveleva, V. Papaefthimiou, M. K. Daletou, W. H. Doh, C. Ulhaq-Bouillet, M. Diebold, S. Zafeiratos and E. R. Savinova, Operando Near Ambient Pressure XPS (NAP-XPS) Study of the Pt Electrochemical Oxidation in H<sub>2</sub>O and H<sub>2</sub>O/O<sub>2</sub> Ambients, *J. Phys. Chem. C*, 2016, **120**(29), 15930–15940, DOI: [10.1021/acs.jpcc.5b12410](https://doi.org/10.1021/acs.jpcc.5b12410).
- 55 E. Herrero and J. M. Feliu, Understanding Formic Acid Oxidation Mechanism on Platinum Single Crystal Electrodes, *Curr. Opin. Electrochem.*, 2018, **9**, 145–150, DOI: [10.1016/j.coelec.2018.03.010](https://doi.org/10.1016/j.coelec.2018.03.010).
- 56 T. Al Najjar, N. Ahmed and E. N. El Sawy, Mechanistic Effects of Blending Formic Acid with Ethanol on Pd Activity towards Formic Acid Oxidation in Acidic Media, *RSC Adv.*, 2021, **11**(37), 22842–22848, DOI: [10.1039/d1ra01209f](https://doi.org/10.1039/d1ra01209f).
- 57 H. Miyake, T. Okada, G. Samjeské and M. Osawa, Formic Acid Electrooxidation on Pd in Acidic Solutions Studied by Surface-Enhanced Infrared Absorption Spectroscopy, *Phys. Chem. Chem. Phys.*, 2008, **10**(25), 3662, DOI: [10.1039/b805955a](https://doi.org/10.1039/b805955a).
- 58 G. Samjeské and M. Osawa, Current Oscillations during Formic Acid Oxidation on a Pt Electrode: Insight into the Mechanism by Time-Resolved IR Spectroscopy, *Angew. Chem.*, 2005, **117**(35), 5840–5844, DOI: [10.1002/ange.200501009](https://doi.org/10.1002/ange.200501009).
- 59 J. Clavilier, Pulsed Linear Sweep Voltammetry with Pulses of Constant Level in a Potential Scale, a Polarization Demanding Condition in the Study of Platinum Single Crystal Electrodes, *J. Electroanal. Chem.*, 1987, **236**(1–2), 87–94, DOI: [10.1016/0022-0728\(87\)88020-8](https://doi.org/10.1016/0022-0728(87)88020-8).
- 60 E. Pizzutilo, S. Geiger, S. J. Freakley, A. Mingers, S. Cherevko, G. J. Hutchings and K. J. J. Mayrhofer, Palladium Electrodeposition from Model Surfaces and Nanoparticles, *Electrochim. Acta*, 2017, **229**, 467–477, DOI: [10.1016/j.electacta.2017.01.127](https://doi.org/10.1016/j.electacta.2017.01.127).
- 61 S. Cherevko, N. Kulyk and K. J. J. Mayrhofer, Durability of Platinum-Based Fuel Cell Electrocatalysts: Dissolution of Bulk and Nanoscale Platinum, *Nano Energy*, 2016, **29**, 275–298, DOI: [10.1016/j.nanoen.2016.03.005](https://doi.org/10.1016/j.nanoen.2016.03.005).
- 62 A. Jain, S. P. Ong, G. Hautier, W. Chen, W. D. Richards, S. Dacek, S. Cholia, D. Gunter, D. Skinner, G. Ceder and K. A. Persson, Commentary: The Materials Project: A Materials Genome Approach to Accelerating Materials Innovation, *APL Mater.*, 2013, **1**(1), 011002, DOI: [10.1063/1.4812323](https://doi.org/10.1063/1.4812323).

